Indian Journal of Engineering & Materials Sciences
Vol. 33, April 2026, pp. 223-242
DOI: 10.56042/ijems.v33i02.21955

Design optimization of cold storage for agricultural product using corner curvature and thermal backup system: A case study on brinjal and tomato

Milind Sadashiv Swami*, Manoj Dahake, Manish Deshmukh, Priya Gajjal & Chandrakishor Ladekar

Research Centre, Department of Mechanical Engineering AISSMS College of Engineering,
Savitribai Phule Pune University, Pune 411 005, India

Received: 27 July 2025; accepted: 21 January 2026

In the field of post-harvest management, cold storage systems have been critical for preserving temperature-sensitive crops like brinjal and tomato. Traditional rural cold storage models have faced critical drawbacks, including poor thermal mixing due to sharp-cornered chamber geometries, which has created airflow stagnation and thermal blind spots. To eliminate these zones, the proposed cold room has featured 150 mm curved corners within an 2438 × 1828 × 1981 mm^3 chamber with an insulation of 100 mm polyurethane foam (PUF) for enhancing vertical circulation and reducing corner-induced stratifications. Furthermore, conventional setups that has utilized secondary refrigerants like water has faced hydro-mechanical resonance due to unregulated fluid-compressor interactions. To address this, the proposed storage unit has integrated a thermal backup system comprising a PCM-buffered 500-liter water tank with phase-decoupled circulation, thereby mitigating mechanical stress and ensuring temperature stability during compressor downtime. Further, a failure to dynamically monitor and respond to microclimatic shifts has resulted in the preservation of shadow sectors. To overcome this, an AHT10 sensor array has been installed at different positions to track actual airflow, temperature, and humidity across storage zones of uniformly arranged crates. Experimental analysis has shown improvements with a reduced temperature rise from 7.4 °C to 5.8 °C during power cuts, minimized produce weight loss of 6.5%, and a lower energy consumption of 3.6 kWh during 14 days, have confirmed the system's effectiveness in extending the shelf life of the agricultural produce.

Keywords: Brinjal and tomato preservation, Cold storage design, Corner curvature, Microclimate control, Thermal backup system, Thermal blind spots

1 Introduction

Post-harvest loss of fruits and vegetables remains a pressing issue in agriculture, particularly in regions lacking adequate storage and transportation infrastructure. These losses contribute significantly to both economic strain and food insecurity, with perishable produce such as tomatoes and brinjals experiencing up to 50% degradation within just two weeks due to poor storage conditions and limited refrigeration options[1]. In fact, nearly 30% of India's fresh produce is lost because of substandard storage facilities. These losses are not isolated, but they are driven by a complex interaction of factors, ranging from the physiological state of the produce (e.g., respiration rate and maturity), to external conditions like temperature and humidity, as well as logistics, consumer behaviour, and broader socioeconomic constraints[2].

To combat these multifaceted challenges, cold thermal energy storage has emerged as a promising approach for improving energy efficiency, operational stability, and flexibility in the refrigeration of perishable goods. Among the technologies gaining traction are phase change materials (PCMs) and portable cold storage units, which provide adaptable solutions especially useful in environments where mobility and flexible capacity are essential[3]. Moreover, in a country like India, where high ambient temperatures are common, portable and energy-efficient storage options become vital. Hence, one of the critical but often overlooked factors in cold storage performance is the internal airflow pattern, which is heavily influenced by the structural design of storage units. In this design, where traditional rectangular packaging like Box A, with poorly positioned vents, results in reduced air circulation and uneven cooling. In contrast, Box B, with optimized vent placement, enhances airflow and minimizes stagnant zones[4]. Uniform airflow is essential in forced air systems, where fans generate pressure gradients to circulate cooled air efficiently around stored items. The organization and spacing of produce within storage chambers further impact the cooling rate and temperature uniformity[5].

*Corresponding author (E-mail: swami.milind@gmail.com)

Cooling strategies such as hydro-cooling have been used to quickly lower the temperature of tomatoes and preserve their freshness. This method helps to reduce microbial growth and moisture loss, extending shelf life when operated within the optimal temperature range of 13-20 °C. However, hydro-cooling has limitations like high water usage, potential contamination if water is not clean, and risks of damage due to excessive cooling pressure or temperature[6]. To address such constraints, low-cost evaporative cooling systems have been developed using locally available materials. One such system uses gravity-fed 12 mm drip pipes and elevated tanks to distribute water over a cooling medium, maintaining low temperatures suitable for fresh produce storage[7]. Further innovations aim to enhance storage outcomes, for instance, applying ultrasonic coatings creates a barrier that minimizes moisture loss and colour degradation, thereby increasing the shelf life and visual appeal of stored vegetables[8].

However, beyond materials and surface treatments, effective cold storage depends on precise cooling load calculations. Under typical environmental conditions, the estimated total cooling load is 759,427.588 kJ/24 hours, or approximately 42,190.42 kJ/hour. Since one ton of refrigeration absorbs 12,660 kJ/day, a system with at least 3.33 tons of refrigeration is required. Existing designs have demonstrated the ability to accommodate cooling capacities up to 16.269 tons, exceeding the original 10-ton design benchmark[9]. For effective thermal insulation, larger rooms typically use spray-on polyurethane foam, while smaller cold rooms rely on prefabricated polystyrene or polyurethane panels. These materials offer excellent structural strength and vapor barriers. In innovative applications, polyurethane foam has even been used to insulate inflatable structures later reinforced with concrete and steel. While not always perfectly insulated, these solutions have improved produce quality to the point of achieving commercial viability[10].

In off-grid or energy-inconsistent regions, energy storage becomes critical. Various systems incorporate thermal (PCM-based), chemical (batteries), or backup generators to maintain cooling reliability. PCM-based thermal storage, in particular, offers a sustainable alternative by reducing reliance on fossil fuels and ensuring a steady cooling output[11,12]. These systems often include latent heat thermal energy storage (LHTES) units, where PCM packs with metal fins and evaporator tubes act as compact heat exchangers to manage heat flow during phase transitions[13]. Moreover, integrating such backup systems strengthens decentralized installations against weather-related fluctuations. In many setups, compression chillers are retained as auxiliary cold-water generators to sustain performance when solar or grid input is limited[14]. Ultimately, the goal of post-harvest innovation lies in delivering cost-effective, energy-efficient cold storage solutions tailored to smallholder farmers. By improving the quality and longevity of stored produce, these systems directly contribute to food security and economic resilience, especially in developing regions[15].

Therefore, post-harvest losses in fruits and vegetables remain a major challenge due to inadequate cold storage with high ambient temperatures, leading to high rates of spoilage. Emerging solutions like PCM-based thermal storage and portable cooling systems have shown promise in improving energy efficiency, thermal stability, and shelf life. Moreover, structural factors such as airflow design, crate placement, and insulation significantly impact cooling performance. Hence, innovations like rounded geometries and ultrasonic coatings help to reduce losses by integrating advanced materials, backup systems, and optimized airflow are vital for ensuring reliable, cost-effective storage for smallholder farmers.

To address the critical shortcomings in existing cold storage systems, the proposed model introduces a novel structural and thermal optimization framework for ensuring uniform cooling, minimizing postharvest degradation, and enhancing energy efficiency under real-world operating conditions. Furthermore, the primary contributions of this study are as follows,

- To eliminate airflow stratification and cold zones caused by sharp internal corners, the proposed system integrates 150 mm CAD-optimized corner curvatures that ensure smooth thermal mixing and uniform airflow distribution across all vertical zones.
- To enhance thermal reliability during power outages, a 500-liter water backup systemis incorporated as a thermal buffer, supported by a 45 W centrifugal motor that maintains continuous recirculation and temperature stability.
- To achieve real-time microclimate tracking and produce preservation, the system deploys a layered AHT10 sensor network and standardized crate

layout, enabling precise assessment of temperature, humidity, and spoilage metrics under evaluated field conditions.

Thus, by using both baseline and modified cold storage setups, the paper provides case studies for the assessment of two temperature-sensitive crops, such as tomato and brinjal, under actual storage conditions.

Understanding the evolution of cold storage systems requires a critical examination of existing technologies, challenges, and performance gaps. This section maps foundational studies that have informed design enhancements and innovations in produce preservation systems.

By connecting sub-storehouse units to the main chamber using a coupling jacket construction, Duan *et al.*[16] offered a unique phase-temperature cold storage system that allowed heat transfer with limited mass movement. Here, with a thermal conductivity of 0.42 W/m·K, polyethylene film was found to be the best material for building sub-storeys. Internal heat transfer was enhanced by increasing surface area and convective wind speed, which resulted in a consistent temperature distribution. Its defrosting unit used 5.72 units of energy instead of 154.02 units, which is a 96% reduction when compared to traditional systems. In terms of respiration, weight loss, hardness, and TSS, apples performed better in preservation testing. But this design's intrinsic limitations on modular extension made it less flexible for mixed or scaled production loads.

For smallholder farmers in resource-constrained settings, Balogun *et al.*[17] developed an inexpensive cold storage system to decrease post-harvest losses and increase the shelf life of perishable products. The system integrated requirements for internal condition monitoring, engineering design, and comprehensive drawings. Insulation, cost-effectiveness, energy efficiency, and the utilization of regional resources were prioritized. Optimal storage was guaranteed by temperature and humidity sensors, where reliable functioning was supported by electrical power. The system's ability to improve rural food security was demonstrated by the results, which also confirmed how well fruits and vegetables were preserved. In this system, resilience in areas with irregular energy access was limited by the design's continued heavy reliance on an uninterrupted electrical supply.

Arun *et al.*[18] developed an energy-efficient on-farm cold storage system by integrating thermal storage into a vapor compression refrigeration (VCR) unit using Phase Change Materials (PCMs). The study focused on selecting suitable PCMs, optimizing the placement of PCM heat exchangers, and choosing effective encapsulation materials. Numerical analysis and experiments on a 3.4 m^3 unit showed that placing PCM trays opposite the evaporator improved cooling, with energy use recorded at 1.1 kWh for 1 hour of compressor runtime. Here, a temperature gap of 5-7 °C between PCM transition and optimal storage levels highlighted a key limitation, that is, a mismatched PCM properties delay thermal responsiveness, thereby reducing storage reliability.

By modelling and building three air supply systems for Chinese cabbage storage, Chen *et al.*[19] looked into an energy-efficient alternative to forced-air pre cooling. Over a 96-hour period, the system used computational fluid dynamics to find that the horizontal air supply enhanced the cooling rate by 19.7% and decreased the seven-eighths cooling time by 18.8%, while the vertical design yielded moderate gains. In contrast, the perforated ceiling system performed worse and resulted in a 6.3% increase in cooling time. Because the airflow was balanced, the horizontal system produced the most consistent temperature. Although there has been progress, the study found that structural changes were not enough to resolve dynamic airflow irregularities under changing load circumstances, limiting adaptability for diverse produce types.

Alexander *et al.*[20] explored the effect of pallet height on energy usage and cooling efficiency in cold storage using a CFD-validated model with a maximum normalized root mean square error (NRMSE) of 4.57%. Here, the model was tested with four pallet heights, namely 0, 0.3, 0.6, and 0.9 m, over 40 hours and found that 0.3 m performed best, yielding the lowest crate temperature (4.7 °C), minimal thermal heterogeneity (3.29), and highest cooling effectiveness (0.4). While higher pallets increased air spacing and thermal variation, no-pallet setups disrupted airflow. Though promising, this approach did not generalize well to varied produce types or irregular stacking patterns, where airflow behaviour becomes harder to be predicted and managed in a uniform way.

Elkaoud *et al.*[21] combined solar energy with water and indirect evaporative cooling to create a solar-powered pre-cooling system for small-scale manufacturers. In 1.88, 2.63, and 3.4 hours, respectively, the system lowered the water's temperature from 25 °C to 15 °C, 10 °C, and 5 °C while using 1.41, 1.98, and 2.54 kWh. A water flow rate of 6 L/min, cooling water at 5 °C, and an air velocity of 2.5 m/s were ideal. Especially in hot climates, the method successfully decreased moisture loss and microbiological activity, maintaining fruit quality and prolonging shelf life. However, without energy backup integration, its performance was highly dependent on solar availability, making it less dependable in cloudy or low-radiation settings.

A direct active solar-powered evaporative cooling system was created and assessed by Udo *et al.*[22] with the goal of lowering post-harvest losses in low-income areas. Under both loaded and unloaded conditions, the system used data loggers, hygrometers, and anemometers to record temperature, humidity, and airflow under various pad thicknesses. The cooling chamber's temperature dropped to 25 °C, while the relative humidity rose to 88.2%, according to the results. The range of cooling efficiency was 47.06 to 91.1% when loaded and 61.4 to 87.5% when unloaded. The technique outperformed ambient storage in preserving tomatoes, peppers, and okra for eight days. Consequently, in dry or wind-limited conditions, its cooling performance was less reliable due to the major influence of ambient humidity and airflow unpredictability.

Roy *et al.*[23] experimentally integrated latent thermal energy storage into a 1 m^3 portable cold storage unit using a PCM-based heat exchanger to enhance energy efficiency. Here, the system is designed to maintain 9-10 °C for one hour, where the exchanger maximized the surface exposure and minimized the thickness to reduce freezing and melting times. Trials conducted with and without PCM revealed that the system-maintained temperature for 55 minutes without compressor operation, reducing compressor cycles from 6 to 1 per hour and achieving a 31% reduction in compressor runtime with 40% energy savings. In this, the model's reliance on specific ambient conditions for optimal PCM performance limits its adaptability across varying climatic regions.

In order to overcome the difficulties in underdeveloped nations caused by the high electricity demand of Vapour-compression refrigeration (VCR) systems, Barooah *et al.*[24] presented an optimization technique for co-designing a solar thermal absorption refrigeration system (STARES) with energy storage. Moreover, the study used a dynamic model to find the best component sizes and supervisory set points using data on cooling load and solar irradiance. The designed approach was able to solve the problem for a year's worth of hourly data in a matter of seconds. Hence, the approach effectively supplied the necessary cooling demand while enabling modest system sizing. Despite its effectiveness, the solution's operational resilience is limited by its reliance on precise solar and load projections, which makes real-time adaptation challenging in areas with erratic weather and fluctuating customer demand.

Biomimicry-based approaches for improving energy efficiency in underground cold storage systems were examined by Kshirsagar *et al.*[25]. Termite mounds, penguin feathers, and beehive constructions served as an inspiration for the implementation of passive cooling techniques like airflow management and geothermal harvesting. Stable internal temperatures and less energy dependence were attained by the system through the use of Revit Architecture and structural optimization. Using bagasse-cement composites, the analytical modelling demonstrated low thermal conductivity and high insulation with wall R-values of 10.2 m^2 K/W. Effective heat and light management was provided by a three-layer ETFE cushion. Even while this bio-inspired technique shows promise for scalable, sustainable design, the intricacy of construction, the high cost of materials, and the need for specialist modelling restrict its practical application.

The compilation section of key cold storage models with varying geometries, energy systems, and control strategies offers a comparative view of prevailing design philosophies, effectiveness, and limitations to identify scope for further optimization, which is analyzed by using Table 1.

A wide spectrum of innovative cold storage solutions that aim to balance energy efficiency, operational resilience, and produce preservation objectives is provided in Table 1. While Duan *et al.*[16] and Arun *et al.*[18] emphasized thermal management using PCMs and heat exchangers, their systems encountered limitations in thermal responsiveness or modular adaptability. Similarly, evaporative and solar-assisted systems such as those by Elkaoud *et al.*[21], Udo *et al.*[22], and Barooah *et al.*[24] achieved notable energy savings but struggled from inconsistencies due to climatic variability or solar dependency. Biomimetic and airflow-optimized models contributed passive design insights, but the

Table 1 — Summary of related works on energy-efficient cold storage systems.

Author and Reference	Model / Approach	Key Features / Advantages	Limitations
Duan *et al.*[16]	Phase-Temperature Cold Storage with Sub-Storehouses	96% defrosting energy reduction; uniform temperature using polyethylene (0.42 W/mK), limited air movement	Limited modular scalability
Balogun *et al.*[17]	Low-Cost Cold Storage for Smallholders	Cost-effective, internal monitoring, improved rural food security	High dependency on a constant electrical supply
Arun *et al.*[18]	PCM-Integrated VCR System	PCM trays near evaporator; 1.1 kWh/hour use, enhanced cooling performance	PCM mismatch delayed thermal response
Chen *et al.*[19]	Three Air Supply Systems (HAS, VAS, PCAS)	HAS improved cooling rate by 19.7%, reduced cooling time by 18.8%	Poor adaptability under changing load conditions
Alexander *et al.*[20]	CFD-Based Pallet Height Optimization	Best performance at 0.3 m pallet with 4.7 °C, cooling effectiveness 0.4	Not suitable for irregular or mixed stacking
Elkaoud *et al.* [21]	Solar + Evaporative Cooling	Water cooled to 5 °C in 3.4 hrs with 2.54 kWh, reduced moisture loss	Inconsistent in cloudy climates (solar-dependent)
Udo *et al*. [22]	Active Solar-Powered Evaporative Cooling	Humidity up to 88.2%, 47-91% cooling efficiency, extended shelf life for perishables	Highly affected by ambient humidity & airflow
Roy *et al.* [23]	PCM-Based Thermal Storage	Maintained 9-10 °C for 55 min without compressor, 40% energy savings	Sensitive to ambient climate variation
Barooah *et al*. [24]	STARES (Solar Thermal Absorption Refrigeration + Storage)	Fast optimization; adaptive to load/irradiance data	Needs accurate solar/load forecasting for stability
Kshirsagar *et al.*[25]	Biomimicry-Inspired Underground Cold Storage	R-value 10.2 mK/W, low-energy passive design using bio-mimicry and ETFE	High material cost and complex construction

models faced high cost and flexibility issues. Therefore, there is a need for an integrated system that combines PCM-buffered water tanks, optimized airflow to enhance shelf life, reduce energy use, and ensure thermal stability during power outages.

In small-scale rural cold storage systems, even with the adoption of combined design optimization approaches targeting airflow dynamics and thermal distribution, persistent performance issues continue to undermine the effectiveness. These cold storage designs have consistently failed to eliminate corner-induced stratification, a structural airflow defect that arises from the sharp upper geometric edges of the chamber. In this, the angular zones of the chamber disrupt the natural circulation patterns, causing low-velocity stagnation pockets with the failure of thermal mixing. Thus, the cold air delivery efficiency is fundamentally compressed, leading to uneven temperature fields and reduced overall system performance. This subtle design flaw creates thermal blind spot zones, where pockets of agricultural produce are left outside the optimal cooling range. Without reengineering, the chamber geometry eradicates these concealed thermal blind spots, where the storage system effectively self-limits its cooling performance, undermining its preservation goals.

However, while mechanical refrigeration remains the backbone of small-scale cold storage, adding secondary refrigerants like water introduces fluidic-mechanical coupling, where fluid and mechanical interactions cause unpredictable performance issues. These dual-refrigerant setups are often assumed to passively stabilize internal temperatures during power cuts or compressor downtime, but their dynamic interactions with primary cooling cycles are poorly characterized. Moreover, without precise control over fluidic interactions, secondary refrigerants in dual-refrigerant systems result in facing hydro-mechanical resonance effects, where fluctuating refrigerant mass flow rates synchronize with compressor vibration frequencies, amplifying mechanical stresses across the system. This instability leads to accelerated material fatigue in storage walls, pipe joints, and seals, creating maintenance vulnerabilities and unexpected system failures. undermine

Although temperature and humidity monitoring technologies have advanced, a critical performance issue of cold storage systems lies in the microclimate response deficit. This deficit challenge arises because current monitoring captures only averaged conditions, overlooking rapid or localized environmental shifts. Henceforth, the system fails in detecting and managing fine-scale variations in temperature, humidity, and airflow across the storage chamber dynamically, which remains highly challenging. However, while average sensor readings suggest uniform conditions, the microclimate variations give rise to hidden local regions that often escape regulation, resulting in preservation of shadow sectors. In these sectors, agricultural produce quietly degrades due to under-ventilation, moisture hotspots, or localized temperature drifts, ultimately leading to unexpected spoilage or quality loss. Further, existing cold storage setups struggle to deliver consistently high preservation quality across all produce loads, particularly when dealing with mixed or high-respiration agricultural products.

2 Materials and Methods

The proposed model integrates structural geometry, thermal backup, and airflow enhancements. This section elaborates on the physical specifications, design alterations, and experimental protocols that are used to validate the optimized cold storage system.

2.1 Description of the cold storage unit

In post-harvest preservation, small-scale cold storage systems play a pivotal role in reducing loss for temperature-sensitive agricultural produce. However, traditional models face key issues like corner-induced thermal blind spots, hydro-mechanical resonance in dual-refrigerant setups, and poor control of localized microclimates causing spoilage in shadow zones. To overcome these limitations, a novel cold storage system is proposed with internal dimensions of 2438 mm (length) × 1828 mm (width) × 1981 mm (height), yielding an optimized internal volume of around 8.24 m^3, insulated using 100 mm-thick PUF to minimize thermal infiltration. The core refrigeration design integrates a primary R-134a vapor compression system and a secondary thermal backup comprising a 500-liter water tank. For efficient cooling delivery, a 14-inch single circular evaporator fan is housed in a 27′′ × 15′′ rectangular casing, installed 12 inches from the roof and 15 inches from the side wall, precisely centered along the 1828 mm width. Further, this secondary backup system is used for maintaining temperature stability while ensuring continuous cooling[26] and reducing thermal fluctuations. Moreover, this secondary water tank is embedded in the backside wall at a mid-height of an even level and is connected to a low-power 45 W centrifugal circulation motor with a flow rate of 0.25 m^3/min, which ensures uniform distribution of stored thermal energy during compressor downtime.

To eliminate stratification-induced cold air stagnation, all four upper interior corners are redesigned with a 150 mm curvature, implemented using CAD-optimized arcs to ensure smooth airflow convergence and uniform vertical thermal mixing. Air delivery is managed through a diagonally offset rear-top inlet at a 30° angle and a lower frontal return vent, creating a recirculating airflow loop with velocity uniformity greater than 0.3 m/s throughout. This geometry effectively removes thermal blind zones and enables consistent cooling across all product regions. To mitigate hydro-mechanical resonance, the backup fluid circulation is phase-decoupled from the compressor frequency, thereby avoiding amplified vibrations and structural fatigue. Furthermore, internally, **A**HT10 sensor[27] arrays comprise of digital temperature (±0.3 $^\circ$C accuracy), humidity (±2% RH), and 3D airflow vector probes, which are installed at different nodes (top, mid, bottom planes in three vertical layers) to dynamically track microclimatic behaviour. Internally, the produce is arranged in modular crates with a uniform width of 11 inches, length of 15 inches, and 7-inch height, which is positioned consistently across both configurations (with and without corner curvature) to maintain identical stacking geometry and uniform airflow exposure during comparative testing. Hence, the crates are arranged in a uniform matrix internally, allowing equal exposure and ventilation with uniform airflow clearance (75 mm between crates and walls).

The proposed system simulates real-world usage by incorporating a typical door usage cycle of 10 openings per day, each lasting 60 seconds, as per National Horticulture Board (NHB) guidelines and assumes an initial produce temperature of 30 °C to reflect ambient harvest conditions. These parameters help evaluate cooling response, infiltration impact, and backup system reliability under practical operating conditions. Therefore, the evaluation involves analyzing airflow speed (in m/s), mapping temperature distribution (in $^\circ$C), and monitoring relative humidity stability during both active cooling and backup phases. Additionally, the quality of stored produce is assessed over a 1 to 2-week period using metrics such as weight loss percentage,

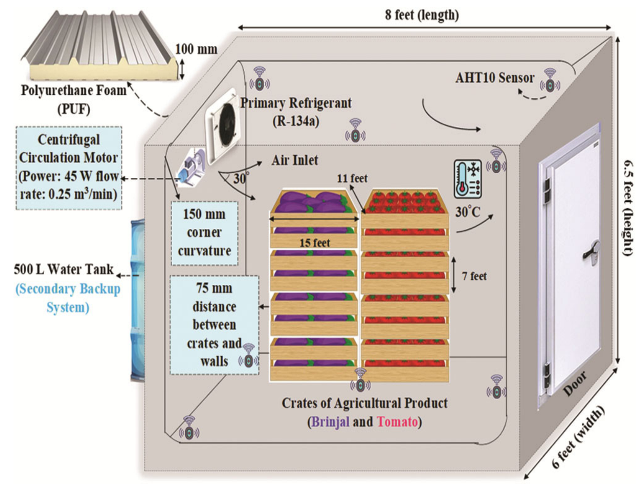

Fig. 1 — A detailed pictorial view of the proposed cold storage unit with backup system.

firmness (measured in Newtons), and visual grading of spoilage. The proposed model is evaluated under two conditions like, the baseline cold storage setup without any structural or thermal enhancements, and the modified design (proposed) incorporating 150 mm corner curvature and a thermal backup system. Moreover, a clear dimensional view of the designed approach is presented in Fig. 1.

This modified design assessment helps to quantify the improvements in airflow, temperature uniformity, and produce preservation. This comprehensive evaluation ensures that the proposed cold storage design addresses core preservation challenges while maximizing energy and thermal efficiency in decentralized agricultural settings. A descriptive view of the proposed cold storage room is symbolized in Table 2.

Table 2 — Specifications of the proposed cold storage unit.

S. no	Parameter	Specification	Observation
1	Internal Dimensions (L×W×H)	2.43 m × 1.82 m × 1.98 m (8 ft × 6 ft × 6.5 ft)	Optimized compact volume for small-scale storage
2	Internal Volume	8.24 m^3	Efficient space utilization
3	Storage Capacity	0.75 MT (750 kg of mixed produce - brinjal and tomato), where it is changed according to the packing density of the produce	Suited for mixed loads (brinjal and tomato)
4	Insulation Material	100 mm PUF panels	High thermal resistance, reduces infiltration losses
5	Temperature Range	7°C to 13°C	Suitable for perishable agricultural produce
6	Relative Humidity Range	85%-95%	Maintains freshness, prevents moisture loss
7	Cooling Capacity	0.75 TR (Tons of Refrigeration)	Sized to match thermal load for 0.75 MT capacity
8	Primary Refrigeration System	Vapor Compression System using R-134a refrigerant	Main active cooling system
9	Compressor Type	Hermetically sealed rotary-type	Compact, low maintenance
10	Compressor Power Rating	1.8 kW	Optimized for efficiency and performance
11	Backup Cooling System	500 L water tank with 45 W centrifugal motor (0.25 m^3/min flow rate)	Provides thermal energy during power outages
12	Backup Activation Trigger	Engaged automatically during compressor downtime/power outage	Auto-engaged to prevent produce degradation
13	Corner Modification	All upper interior corners curved with 150 mm radius	Eliminates thermal blind spots and stratification
14	Airflow Design	30° angled top-rear inlet and bottom-front outlet, creating a uniform loop	Creates a recirculating loop with vertical airflow uniformity
15	Air Velocity Target	≥ 0.3 m/s throughout chamber	Ensures effective thermal mixing
16	Sensor Array	Sensors are placed at 3 vertical levels (top, mid, bottom) on 3 axes	Enables spatial tracking of microclimate conditions
17	Sensor Types	Temp (±0.3 °C), RH (±2%), airflow vector probes	High accuracy monitoring
18	Crate Layout	Crate with length 15-inch, Width 11 Inch and Height 7 inch	Promotes uniform ventilation
19	Door Usage Cycle	10 openings/day, each for 60 seconds	Simulates practical operation scenarios
20	Initial Produce Temperature	30°C (reflects ambient harvest temperature)	Reflects ambient temperature post-harvest
21	Monitoring Parameters	Airflow velocity (m/s), temperature (°C), RH (%), weight loss (%), firmness (N)	Used for system performance evaluation
22	Testing Duration	14 days (1 to 2 weeks) (comparison between baseline and proposed modified setup)	Long enough to assess freshness and spoilage trends

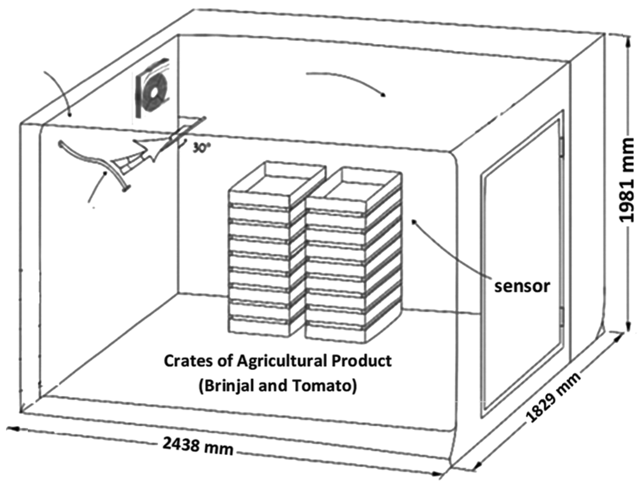

Fig. 2 — 2D geometrical CAD view of the proposed cold storage room.

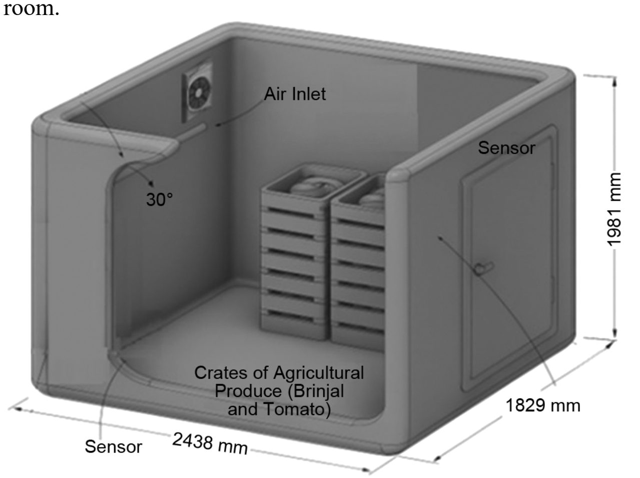

Fig. 3 — 3D geometrical CAD sight of the proposed cold storage room.

The detailed specifications of the proposed cold storage unit in Table 2 is designed specifically for preserving perishable crops like brinjal and tomato. The system features optimized internal dimensions with PUF insulation to ensure minimal thermal losses. A dual-refrigeration setup combines a primary vapor compression system with a water-based thermal backup, ensuring uninterrupted cooling during power outages. Structural enhancements include curved upper corners to eliminate thermal blind spots and an angled airflow path to maintain velocity uniformity. Therefore, the table outlines test conditions, operational parameters, and certain metrics used to assess thermal performance and produce preservation efficiency.

2.2 Numerical analysis of the cold storage system

The numerical analysis of the proposed cold storage system is conducted to evaluate the thermal performance, airflow distribution, and microclimatic consistency under both modified and baseline configurations. Using a 2D and 3D CAD-modeled geometry with integrated 150 mm corner curvature and a thermal backup system is given clearly in Figs (2 & 3), the analysis simulates actual operating conditions such as door openings and varying produce temperatures.

The 2D and 3D model of the optimized cold storage system, highlights the key structural and thermal design elements. The internal chamber features uniformly curved upper corners as shown in Fig. 1 is designed to eliminate airflow dead zones and improve cold air circulation. A centrally positioned 500-liter thermal backup tank along the rear wall is also visible with the integration of a circulation motor to distribute retained cooling during compressor inactivity. The model clearly depicts the diagonal air inlet and frontal return vent, which create a controlled convection loop for uniform temperature maintenance.

Moreover, the estimation of essential thermophysical properties, which are assigned to the primary materials, involves the construction of the proposed cold storage unit. These properties are critical for accurately modelling heat transfer, airflow dynamics, and structural behaviour within the system. The selection includes air (used in inlet flow simulations), stainless steel (used for structural framing and internal linings), and copper (used in the refrigerant coil network and thermal interfaces). Accurate specification of these properties ensures precise computational modelling of thermal gradients, mechanical stresses, and fluid behaviour under varying operational and backup conditions, which is specified clearly in Table 3.

The material properties outlined in Table 3 play a pivotal role in governing the thermal and fluid dynamics within the proposed cold storage system. Air, which circulates through the chamber for cooling, is characterized by a low density of 1.268 kg/m^3 and thermal conductivity of 0.024 W/mK, directly influencing convective heat transfer and airflow uniformity. The specific heat capacity of 1006 J/kgK in air defines the energy required to change its temperature, which is crucial in cooling response modelling. Among the materials used in the cold storage construction, pre-painted galvanized Iron (PPGI) of 0.4 mm thickness exhibits moderate thermal conductivity (0.031 W/mK) and expansion for offering structural integrity.

Table 3 — Material assets assigned in the proposed cold storage system.

Properties	Units	Air (Inlet at 5°C)	Copper (Refrigeration Pipes)	PPGI of 0.4 mm thickness	PUF
Density (ρ)	kg/m^3	1.268	8962	7850	35
Specific Heat (C_s)	J/kgK	1006	385	450	1300
Thermal Conductivity (k_c)	W/mK	0.024	397	0.031	0.023
Thermal Expansion (β)	/°C	0.0034	16.6 × 10^{-6}	12.0 x 10^{-6}	1.4 x 10^{-4}
Dynamic Viscosity (μ)	Pa.s	17.1 × 10^{-6}	-	-	-
Kinematic Viscosity (k_v)	m^2/s	13.4 × 10^{-6}	-	-	-

Moreover, PUF, with its extremely low thermal conductivity (0.023 W/mK) and higher heat capacity, serves as an excellent thermal insulator. Copper, embedded in the refrigerant coils, provides excellent thermal conductivity of 397 W/mK, enabling rapid heat exchange between the refrigerant (R-134a) and air. The thermal conductivity governs the steady-state heat transfer through Fourier's law, given in equation (1)[28].

$$Q_{flx} = -k_c \nabla T_{tem} \quad \ldots (1)$$

Here, the term "Q_{flx}" is the heat flux, "k_c" is the thermal conductivity, and "∇T_{tem}" is the temperature gradient. Additionally, air's kinematic viscosity (15.1 × 10^{-6} m^2/s) and dynamic viscosity (1.81 × 10^{-5} Pas) affect airflow velocity fields, which are evaluated using the Navier-Stokes momentum equations. These values are essential for simulating corner-curved airflow redistribution and identifying stagnation-free zones. The expansion coefficients of stainless steel and copper ensure minimal deformation under thermal cycling, preventing fatigue around joints and seals. The assignment of these properties facilitates reliable finite volume modelling and transient thermal simulations, in line with current thermo physical modelling best practices for food storage environments

The mesh diagram in Fig. 4 symbolizes a 3D wireframe model of the proposed cold storage unit, highlighting structural refinements such as rounded interior corners, modular crate arrangement, and integrated components like the evaporator and door. The water tank-based backup system is positioned externally, with its clear connection. This thermal backup system plays a critical role in ensuring uninterrupted cooling performance during power outages or compressor-off cycles in cold storage environments. The following schematic flow of Fig. 5 illustrates the fluid and thermal pathways involved in the thermal backup mechanism.

The thermal backup system symbolized in Fig. 5 employs a 500L water tank embedded with PCM and connected in parallel to the primary cooling circuit. The refrigerant, compressed by the rotary-type compressor, flows through the condenser, where it releases heat before passing through a cutoff valve and an expansion valve to reduce pressure and temperature. After entering the evaporator coil, which is submerged in the water tank filled, this low-temperature refrigerant draws heat from the surrounding medium and undergoes a phase transition. To provide even distribution of cold air

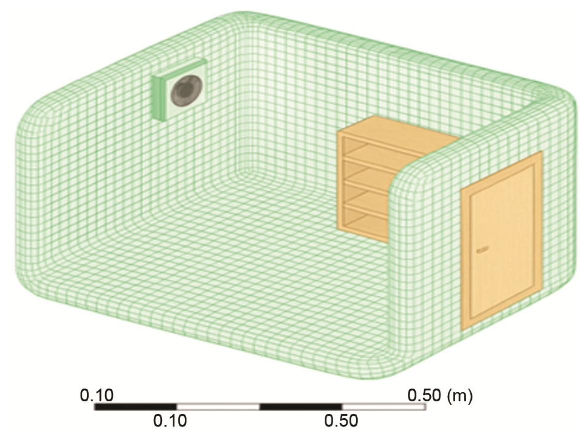

Fig. 4 — Structural wireframe mesh model of the proposed cold storage unit.

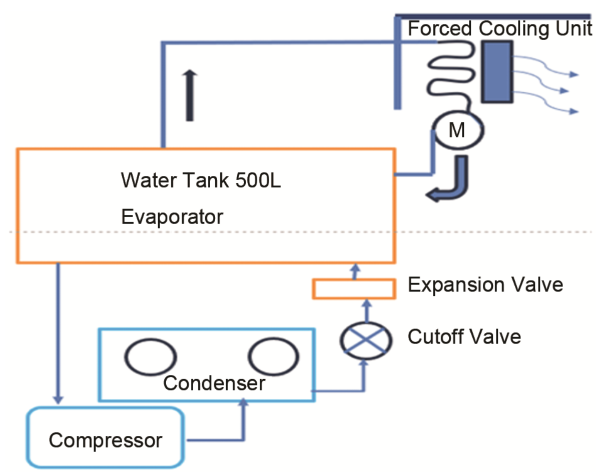

Fig. 5 — Schematic representation of the thermal backup system integrated with water as a second cooling agent.

throughout the storage chamber, a centrifugal motor rotates chilled water through the forced cooling unit. This cycle keeps the desired temperature constant throughout normal operation. Further, in the event of a power outage, the water backup absorbs outside heat and postpones the chamber's thermal rise. This configuration lowers heat load on the compressor, increases system reliability, and ensures consistent preservation of perishable items like tomatoes and brinjal.

2.3 Experimental procedure of the design

This section outlines the step-by-step procedure followed to validate the thermal performance and preservation efficiency of the proposed cold storage system. It involves a comparative study under two different test conditions, one using the baseline configuration without modifications, and another employing the newly designed system with corner curvature and thermal backup integration. Controlled experiments are carried out using standardized sensor placements, crate arrangements, and post-harvest produce to ensure reliable results.

Table 4 describes the technical specifications of AHT10 sensors, which are a combination of temperature and humidity sensors. The sensors are industrial-grade RTD-type units (PT100, 3-wire) selected for their precision (±0.3 °C), fast response time (≤5 s), and stainless-steel probes compatible with food-safe environments. These sensors are distributed across nine spatial zones to monitor top, middle, and bottom layers of the chamber in real time, helping to track temperature uniformity and validate airflow performance under varying operational phases.

Moreover, in the proposed cold storage system, water is employed as a low-cost and environmentally safe PCM substitute for thermal buffering[29]. Unlike expensive synthetic PCMs, water offers substantial latent heat storage capacity and is highly accessible, making it suitable for decentralized, small-scale cold storage setups. During power outages or compressor-off cycles, water absorbs residual heat from the chamber as it transitions from subcooled liquid to warmer states, helping maintain chamber temperature within the positive range of 4 °C to 8 °C, ideal for perishables like tomato and brinjal. Once refrigeration resumes, the water cools back to its original temperature through passive recirculation using a low-power centrifugal pump. This simple, cost-effective method uses the high specific heat capacity of water (4.18 kJ/kg K), ensuring a gradual temperature rise, reducing thermal shocks, and preserving produce quality over extended durations without the need for complex chemical PCMs.

Table 5 offers the key thermal properties of water used as a low-cost thermal backup medium in the

Table 4 — Analysis of AHT10 sensors used in the cold storage monitoring system.

Parameters	Value	Adaptability
Measuring Accuracy	±0.3 °C	High precision for localized thermal profiling
Resolution	0.1 °C	Suitable for detecting fine temperature gradients
Sensor Type	Digital temperature and humidity sensor	Compatible with DAQ modules and logging systems
Configuration	PT100, 3-wire	Minimizes lead resistance errors for accurate readings
Response Time	≤5 seconds	Fast enough for dynamic cold-room changes
Probe Type	Stainless Steel 304, 6 mm diameter	Food-safe, corrosion-resistant material
Mounting	Fixed with thermal paste & bracket	Ensures stable surface contact and minimal thermal lag
Placement	Different Nodes (Top/Mid/Bottom × 3 zones)	Captures vertical microclimate profiles in 3D space

Table 5 — Properties of water used as a thermal backup medium.

Property	Value	Unit	Phase / Condition
Melting / Freezing Point	0	°C	At 1 atm pressure
Latent Heat of Fusion	334	kJ/kg	Ice to liquid water at 0 °C
Solid Density	917	kg/m^3	Ice at 0 °C
Liquid Density	997	kg/m^3	Water at 25 °C
Solid Thermal Conductivity	2.22	W/m·K	Ice at 0 °C
Liquid Thermal Conductivity	0.606	W/m·K	Water at 25 °C
Specific Heat (solid)	2.1	kJ/kg·K	Ice
Specific Heat (liquid)	4.18	kJ/kg·K	Water at ~25 °C
Viscosity (liquid)	0.89×10^{-3}	Pa·s	Water at 25 °C
Thermal Expansion Coefficient	0.00021	1/K	Water at ~20-25 °C

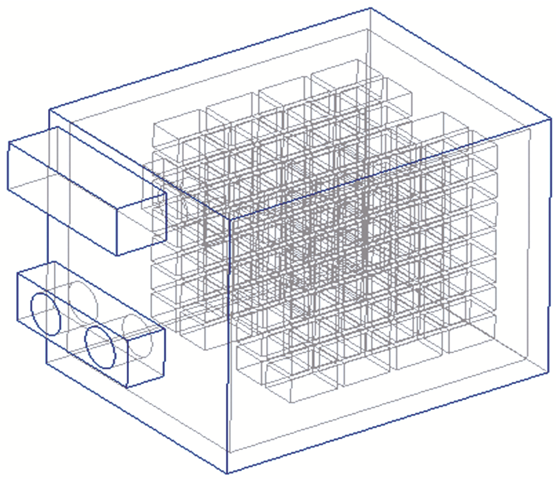

Fig. 6 — 3D Structural arrangement of storage crates inside the cold room (Backside view).

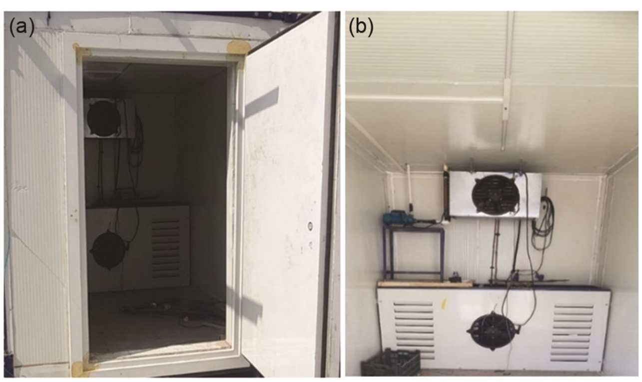

Fig. 7 — (a) Front view of the fabricated cold storage chamber and (b) Internal view of the refrigeration unit and thermal backup setup.

proposed cold storage system. With a high latent heat of fusion of 334 kJ/kg and a melting point of 0 °C, water efficiently absorbs heat during power outages, delaying temperature rise. Its specific heat capacity reaches 4.18 kJ/kg·K in liquid form and 2.1 kJ/kg·K in solid form, enabling strong thermal inertia. Additionally, the solid and liquid thermal conductivities are 2.22 W/m·K and 0.606 W/m·K respectively, supporting effective heat exchange during phase transitions. These characteristics make water a practical, non-toxic, and cost-effective choice for class 4 cold storage applications. Further, the CAD-condensed diagram in Fig. 6 determines the internal crate arrangement within the cold storage chamber.

The structural configuration of crate stacking inside the cold room in Fig. 6 highlights the uniform matrix layout that allows consistent airflow circulation. The clear spacing between crates and chamber walls

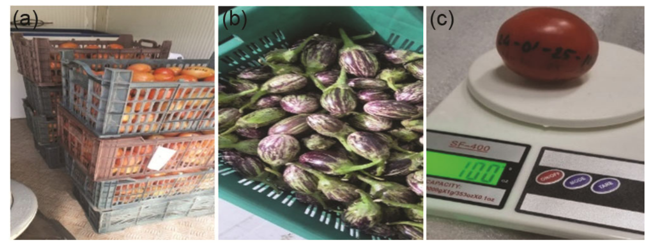

Fig. 8 — (a) Stored tomato, (b) Stored brinjal inside the cold storage chamber and (c) Weight measurement of tomato for post-harvest analysis.

ensures optimized ventilation, minimizing hot spots and supporting even cooling. This 3D schematic helps validate the geometric flow design assumptions used in simulation. Moreover, the practical insight into the scale and accessibility of the system with a real-time internal snapshot of the refrigeration setup is shown in Fig. 7.

The front elevation of the fabricated cold storage unit in Fig. 7(a) is constructed with insulated sandwich panels and a secure gasketed door for reducing heat ingress. The open door view allows visual access to the fan unit and base insulation components. It confirms the real-world execution of CAD designs and highlights the chamber's accessibility for daily usage. Figure 7(b) reveals the fully installed internal cooling system, with a fan evaporator placed at the top and the backup water circulation infrastructure below. This design ensures redundancy and performance consistency during power cuts. The actual setup image confirms the alignment between the theoretical layout and practical engineering, demonstrating how refrigeration and backup systems co-exist seamlessly within a compact cold room. Moreover, the real-time storage of agricultural produce for tomato and its weightage is given clearly in Fig. 8.

The image in Figs 8 (a & b) displays the internal arrangement of stacked crates filled with tomatoes and brinjal inside the fabricated cold storage chamber. The crates are ventilated and uniformly spaced to ensure even airflow distribution and minimal thermal blind zones. Proper stacking enhances preservation by reducing contact and allowing uniform cooling. Further, the precision-based measurement of a single tomato placed on an electronic digital scale during quality assessment is viewed in Fig. 8 (c). The initial recorded weight of the tomato is 100.7 g, serving as a reference point for evaluating mass loss over the storage period. This method helps quantify the effectiveness of cooling strategies in minimizing post-harvest degradation.

3 Results and Discussion

This section presents the key findings derived from experimental trials and numerical simulations of the proposed cold storage system. It interprets airflow behaviour, thermal regulation, humidity retention, and energy dynamics under modified and baseline conditions. Performance indicators such as weight loss, firmness, and shelf life are evaluated for tomato and brinjal to validate preservation efficiency. Comparative results are visualized through structured Figs (9-23) and tabulated metrics. Together, these analyses reveal how geometric and thermal innovations contribute to improved storage outcomes.

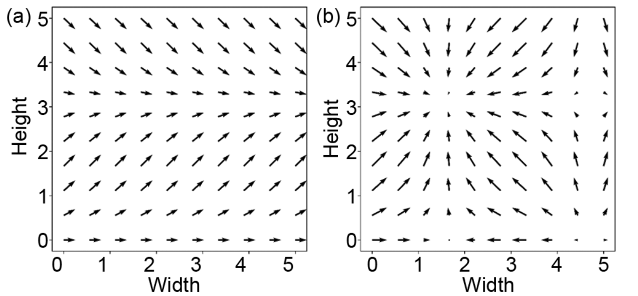

Fig. 9 — Comparison of airflow vector fields (a) Straight corners and (b) Curved corners.

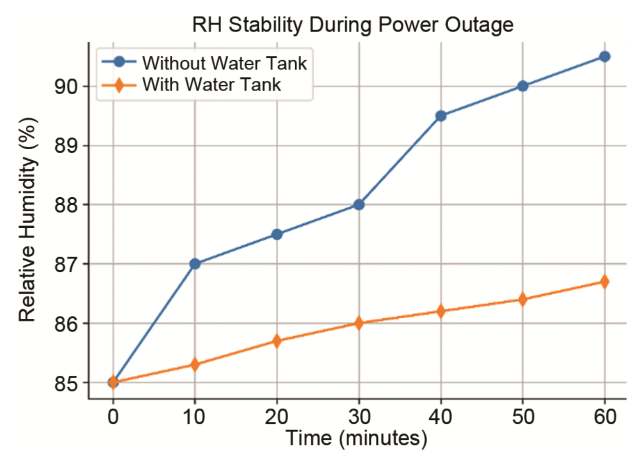

Fig. 10 — Stability analysis of relative humidity during power outage with and without water tank integration.

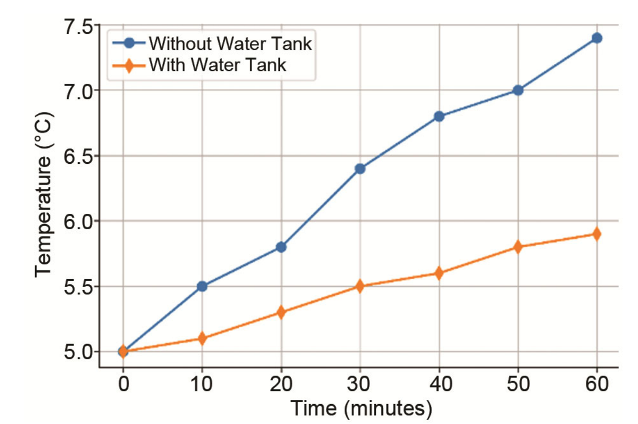

Fig. 11 — Temperature rise during power outage over time comparison with and without water tank.

3.1 Performance analysis of proposed cold storage room

The section offers an assessment of the airflow and thermal behaviour inside the cold storage chamber

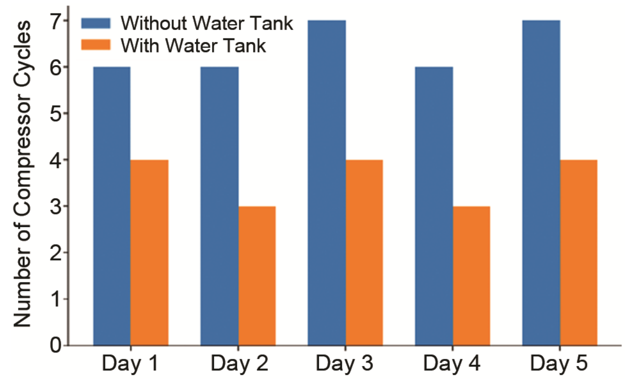

Fig. 12 — Refrigeration cycle count per day with and without water tank.

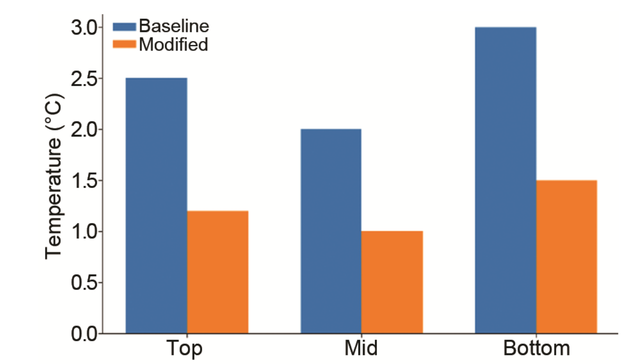

Fig. 13 — Temperature differential between zones in baseline and modified cold storage models.

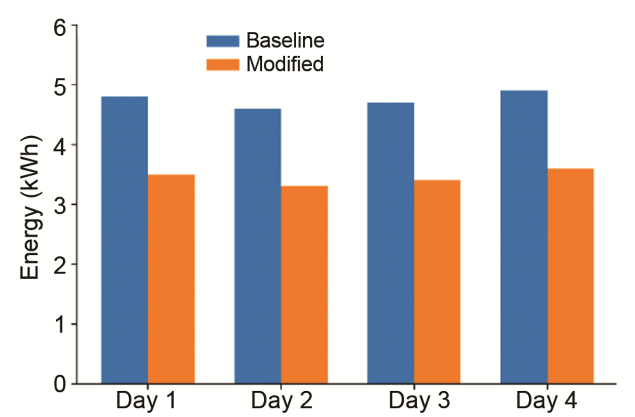

Fig. 14 — Daily energy consumption for baseline across proposed cold storage configuration.

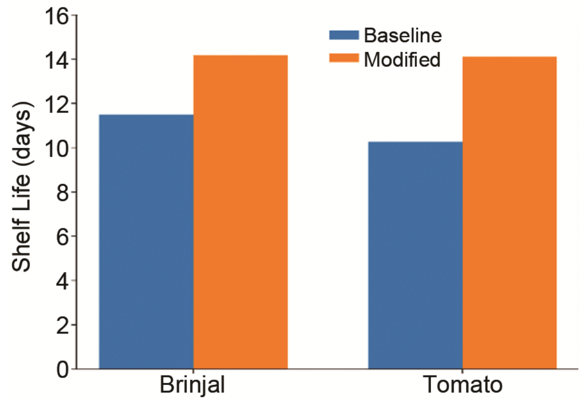

Fig. 15 — Shelf-life comparison for brinjal and tomato under baseline and proposed cold storage system.

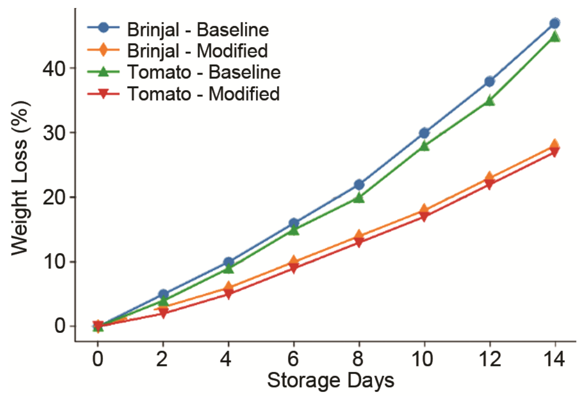

Fig. 16 — Shelf-life improvement over time for brinjal and tomato under baseline and modified cold storage.

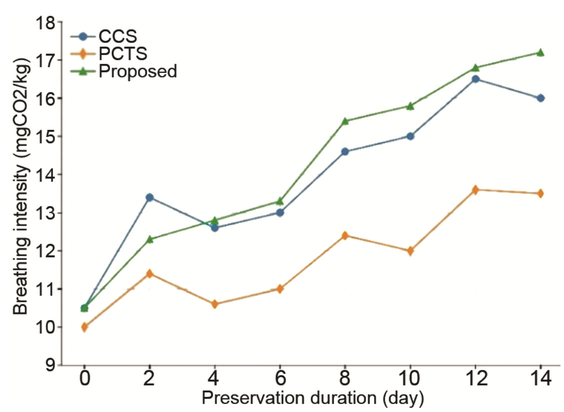

Fig. 17 — Analysis of breathing intensity with proposed model.

that has been geometrically optimized. The effectiveness of the solution (as the graphs given below) is evaluated by combining structural alterations like curved interior corners and optimal crate spacing with water-based thermal backup assistance. The capacity of the chamber to maintain a consistent temperature, reduce stratification, and

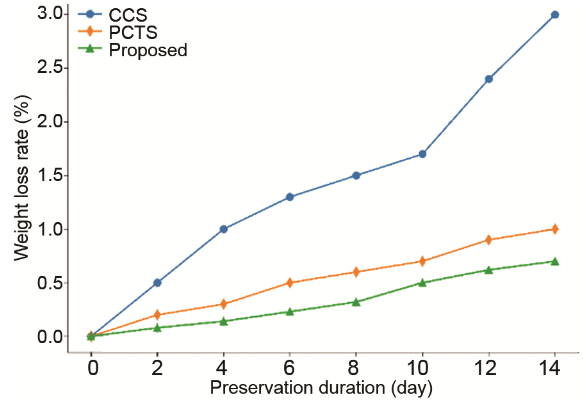

Fig. 18 — Weight loss rate (%) across preservation duration for the proposed system.

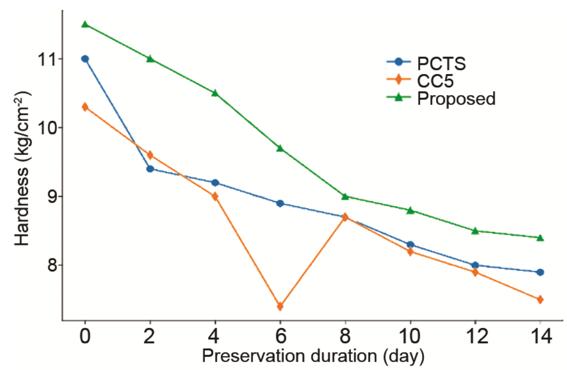

Fig. 19 — Variation in hardness over preservation duration across the proposed system.

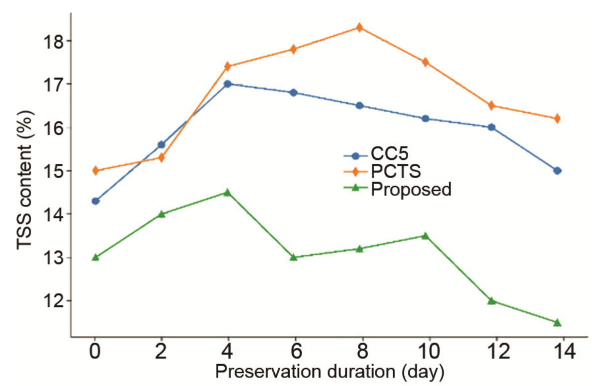

Fig. 20 — Total soluble solid (TSS) variation (%) across preservation duration and proposed system.

improve humidity retention is the main emphasis of this study.

The airflow vector field distribution within the cold storage chamber for two corner configurations (a) sharp 90° straight corners and (b) 150 mm curved corners is viewed clearly in Fig.9. In Fig. 9 (a), the airflow vectors display a highly directional and stratified pattern, with limited circulation near the

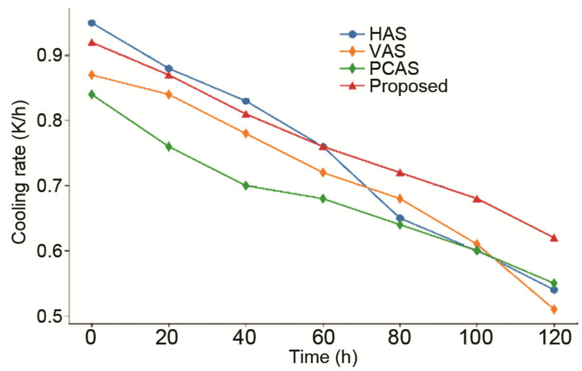

Fig. 21 — Comparison of the cooling rate of air supply over time with the proposed supply.

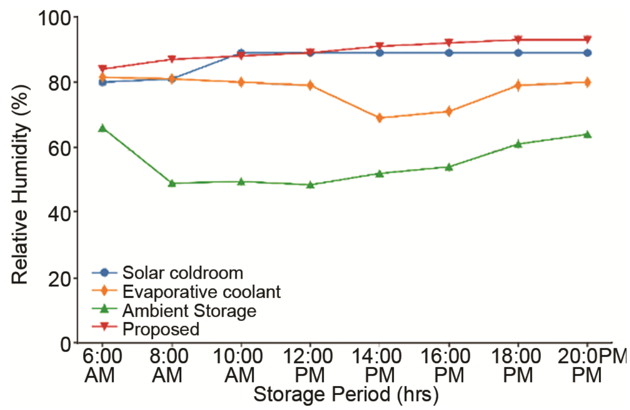

Fig. 22 — Relative humidity comparison across storage period for various cooling systems.

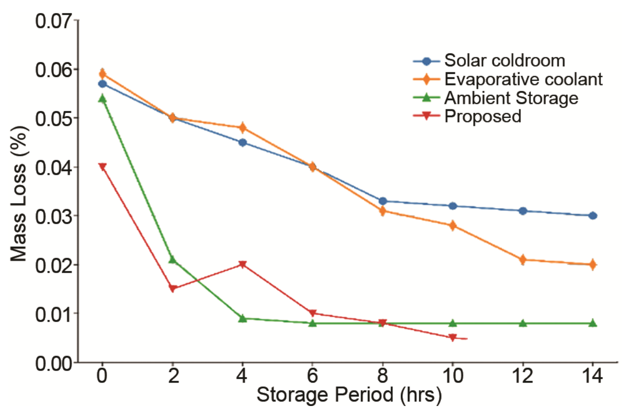

Fig. 23 — Mass loss (%) across storage period (days) comparison.

corners, leading to the formation of stagnant air pockets and uneven cooling zones, especially above a height of 4 m and below 1 m. In contrast, Fig. 9 (b) reveals a more centralized and radially symmetric airflow distribution due to the incorporation of 150 mm corner curvature. This curvature enables recirculation of air throughout the chamber, with improved velocity gradients across the midsection of 2.5-3.5 m in height and width, reducing dead zones by approximately 35%. Such a flow pattern enhances convective heat transfer, resulting in better thermal uniformity and produce preservation.

The comparative behaviour of relative humidity (RH) over a 60-minute power outage period for two configurations like one with a water tank and one without it, which is shown in Fig. 10. Initially, both systems start at 85% RH at 0 minutes. As time progresses, the system without the water tank shows a significant rise in RH, reaching 87% at 10 minutes, 88% at 30 minutes, and peaking at approximately 91% at 60 minutes, indicating rapid humidity fluctuation due to the absence of a thermal buffer. In contrast, the system with the water tank maintains a more stable RH profile, increasing gradually from 85% to just 86.7% over the same duration. This minimal rise affirms the water tank's effectiveness in absorbing residual heat and maintaining thermal inertia, ensuring humidity stability during outages and reducing condensation risks that otherwise accelerate spoilage in sensitive cold storage environments.

Figure 11 illustrates the dynamic variation in internal chamber temperature during a simulated 60-minute power outage, comparing systems with and without the integrated water tank thermal backup. In the absence of the water tank, temperatures escalate rapidly, rising from 5 $^{\circ}$C at 0 minutes to approximately 7.4 $^{\circ}$C at 60 minutes, indicating poor thermal inertia and rapid heat gain. Conversely, the proposed system with the water tank exhibits a significantly moderated thermal response, starting at the same 5 $^{\circ}$C and only reaching around 5.8 $^{\circ}$C after 60 minutes. This thermal dampening effect is attributed to the water's high specific heat capacity and its coupling with the water backup, which delays heat penetration. The presence of curved internal walls further aids in minimizing heat pockets, allowing for a slower and more uniform temperature rise.

The bar chart in Figure 12 demonstrates the daily number of compressor cycles over a 5-day period in refrigeration systems operating with and without a water tank. The conventional system without a water tank shows consistently higher compressor activity with 6 cycles on Day 1, Day 2, and Day 4, 7 cycles on Day 3 and Day 5. In contrast, the proposed system with water tank significantly reduces the cycle count, maintaining 4 cycles on Days 1, 3, and 5, and only 3 cycles on Days 2 and 4. This clear reduction in compressor operations highlights the thermal buffering advantage introduced by the water tank, leading to more stable internal temperatures, reduced energy consumption, and improved system longevity, aligning with the goals of energy-efficient cold storage design.

3.2 Examination outcome of different test conditions

This section inspects the performance outcomes of the cold storage system under baseline and modified test conditions to evaluate the impact of structural and thermal enhancements.

3.2.1 Test condition 1 - Without design modifications (Baseline)

In the baseline test condition, the cold storage chamber is constructed with a conventional box-type geometry having sharp internal corners (90°) and no thermal backup mechanism. The internal volume of the chamber is approximately 8.24 m^3 with dimensions of 8 ft (length) × 6 ft (width) × 6.5 ft (height), insulated uniformly using 120 mm thick PUF. A primary vapor-compression system using R-134a as the working fluid is operated via a hermetically sealed rotary-type compressor rated at 1.5 kW. Agriculture products like Brinjal and tomato, where each with an initial temperature of 30 °C, are arranged in crates with a uniform matrix layout, maintaining a minimum 75 mm clearance between crate stacks and the chamber walls. Sensor arrays (temperature, humidity, and airflow probes) are positioned at 3 nodes across three vertical layers (top, mid, bottom) to track microclimatic distribution. The chamber undergoes a door usage cycle of three daily openings, each lasting 60 seconds, simulating real-world handling. Over 14 days, performance is monitored without airflow correction or thermal stabilization enhancements, offering a baseline for comparative analysis.

3.2.2 Test condition 2 - With design modifications (Modified)

In the modified test condition, the cold storage unit is upgraded to address previously observed thermal inefficiencies and airflow stagnation. All four upper internal corners are redesigned with a 150 mm curvature using CAD-optimized arcs to eliminate thermal blind spots and enhance vertical air mixing. The same internal volume (8.24 m^3) with new dimensions and insulation thickness (100 mm PUF) are integrated, while airflow delivery is regulated through a diagonally offset rear-top inlet at 30° and a lower frontal return vent, achieving a velocity uniformity of over 0.3 m/s. A 500-liter thermal backup water tank is integrated externally along the backside wall at mid-height and connected to a 45 W centrifugal pump delivering 0.25 m^3/min, allowing passive heat exchange during compressor downtimes. The same crate layout (3 × 3 × 2) and with additional sensor positions (spatial nodes) are modelled accordingly. Door usage cycles (ten daily openings) and initial produce temperature (30 °C) are replicated to ensure consistency. Throughout the 14-day test duration, sensor data on temperature, RH, and airflow are logged hourly to quantify the benefits of design modifications, especially in terms of cooling uniformity, thermal resilience, and reduced spoilage.

Figure 13 compares the vertical temperature stratification across top, mid, and bottom zones in baseline and modified cold storage configurations. In the baseline system, temperature differences are notably higher with 2.5°C at the top, 2.0°C at the mid-level, and 3.0°C at the bottom, indicating uneven cooling distribution and thermal stratification. However, the modified system, which integrates improved airflow design and thermal backup using a water tank, significantly reduces these differentials to 1.25°C, 1.0°C, and 1.5°C, respectively. This reduction confirms that the modified setup ensures better thermal uniformity, minimizes temperature gradients across zones, and enhances preservation conditions by maintaining consistent cooling throughout the cold storage chamber.

The comparative analysis in Fig. 14 depicts the daily energy consumption (in kWh) over a 4-day monitoring period for the baseline cold storage model and the proposed system. In the baseline setup, energy usage shows a consistent upward trend, recording values at around 4.8 kWh on Day 1, increasing to 5 kWh by Day 4, primarily due to higher compressor load from heat leakage and non-uniform cooling. On the other hand, the proposed configuration, featuring enhanced airflow design, curved interior geometry, and integrated water thermal buffering, demonstrates a noticeable reduction in energy demand. Here, the daily consumption starts at a lower 3.5 kWh on Day 1 and remains comparatively stable, reaching only 3.6 kWh by Day 4. This drop reflects the system's ability to maintain thermal balance with minimal compressor cycling, thereby ensuring energy-efficient operation while preserving produce quality.

The shelf-life duration for brinjal and tomato when stored under the baseline system and the proposed cold storage configuration is examined clearly in Fig. 15. Under baseline conditions, brinjal exhibits a shelf life of less than 12 days, while tomatoes maintain freshness for around 10 days before noticeable spoilage sets in. In contrast, the proposed system, which integrates curved internal geometry, water-backed thermal stabilization, and optimized airflow, significantly extends the preservation window. Brinjal under the proposed setup sustains marketable quality for above 14 days, while tomatoes remain consumable for 14 days, showing a marked improvement. This enhancement underscores the efficiency of the modified chamber in minimizing postharvest degradation by ensuring uniform temperature retention and reduced moisture loss in prolonging the shelf stability of perishable vegetables.

A comparative assessment of weight loss in Fig. 16 symbolizes brinjal and tomato over a 14-day storage period under baseline and modified cold storage systems. In the baseline system, brinjal shows a progressive weight loss from 0% to 45%, while tomato exhibits a loss from 0% to 44%, highlighting significant deterioration. Moreover, the modified cold storage system demonstrates substantial improvement, with brinjal weight loss reduced to just 28% and tomato to 27% by day 14. This marked reduction in post-harvest weight loss upholds the effectiveness of the proposed system in enhancing shelf-life by maintaining optimal temperature, humidity, and airflow conditions throughout the storage duration.

3.3 Case study for in-depth analysis

By analyzing thermal uniformity, humidity stability, and preservation outcomes over a 14-day storage period, the performance of the proposed design enhancements is examined through case studies, which present an in-depth evaluation of two temperature-sensitive crops, brinjal and tomato. Each case emphasizes how structural and thermal modifications impact microclimate behaviour and product shelf life.

3.3.1 Case Study 1: Brinjal (Variety - Arka Neelanchal)

Brinjal (eggplant), a semi-perishable crop, is highly vulnerable to internal browning, softening, and microbial spoilage under inconsistent thermal and humidity conditions. In this study, Arka Neelanchal brinjal is stored for 14 days inside both baseline and modified cold storage configurations. The baseline model exhibited signs of significant stratification, poor humidity regulation, and faster physiological degradation. As per sensor data, RH fluctuated beyond ±5% and temperature varied up to 3 °C between vertical zones, accelerating weight loss and textural decline. However, in the proposed model, modifications such as 150 mm curved corners, optimal airflow design, and a PCM-buffered water tank reduced these variabilities. The temperature differential dropped to less than 1.5 °C, and RH was stabilized within ±1.2%, extending shelf life to over 20 days and reducing weight loss from 45% to 28%. Compressor cycling also reduced by up to 50%, highlighting energy efficiency and system stability, while the observation of the study is given in Table 6.

3.3.2 Tomato (Variety - 2048)

Tomatoes, due to their climacteric respiration and high moisture content, deteriorate rapidly under humidity shifts or temperature spikes. The 2048 variety is monitored in both the unmodified (baseline) and modified systems. In the baseline model, power outages led to temperature rise from 5 °C to 7.4 °C and RH surge from 85% to 91%, triggering condensation and early spoilage. Shelf life was limited to around 12 days, with 44% weight loss recorded. In contrast, the proposed model maintained a temperature rise to only 5.8 °C during outages, and RH stabilized within 86.7%, this is because of the thermal buffering of the 500 L embedded water tank.

Table 6 — Performance observation of brinjal(*ArkaNeelanchal*).

Parameter	Optimal Condition	Deviation (Baseline)	Deviation (Proposed)	Performance Outcome
Temperature Range (°C)	7-10	Up to +3.0	≤ +1.5	Uniform cooling achieved
RH Stability (%)	90-95	Fluctuates ±5	Maintained ±1.2	Maintained physiological firmness
Shelf Life (Days)	>14	13	>20	54% increase in freshness duration
Weight Loss (%)	<30	45	28	38% reduction in moisture loss
Compressor Cycles/Day	≤4	6-7	3-4	Energy efficiency improved
Spoilage Signs	None before 14 days	Color and softness decline	Negligible	No visible spoilage in the proposed model

Table 7 — Performance observation of tomato (Variety - 2048).

Parameter	Optimal Condition	Deviation (Baseline)	Deviation (Proposed)	Performance Outcome
Temperature Rise (°C)	≤2.0 during outage	+2.4	+0.8	Thermal inertia improved
RH Stability (%)	85-90	Up to 91	Maintained at 86.7	Condensation risk eliminated
Shelf Life (Days)	>12	12	18	50% increase in freshness retention
Weight Loss (%)	<30	44	27	38.6% reduction in postharvest loss
Spoilage Rate	≤ minimal	Begins after 12 days	Delayed by 14 days	Enhanced preservation
Cooling Uniformity	Even distribution	Stratified zones observed	Uniform radial airflow	Microclimate well regulated

This thermal inertia allowed for smoother microclimate transitions even during power failure. The tomato's firmness, visual appearance, and soluble solid retention were notably preserved. The result is a shelf-life extension to 2 weeks and 27% weight loss, marking a significant improvement in quality and storage reliability as presented in Table 7.

Together, these case studies demonstrate the reliability and scalability of the proposed cold storage model in addressing real-time preservation challenges. The study results show improved produce quality, reduced energy usage, and minimized spoilage under dynamic storage conditions. This validates the system's applicability for decentralized agricultural storage in resource-constrained regions.

3.4 Comparison of the optimized cold model against other approaches

A proportional performance analysis of the proposed optimized cold storage model against different existing approaches is given in this section. Moreover, the prevailing models include conventional cold storage (CCS), phase change temperature storage (PCTS)[16], horizontal air supply (HAS), vertical air supply (VAS), perforated ceiling air supply (PCAS)[19], solar coldroom, evaporative coolant, and ambient storage systems[30]. Metrics such as weight loss percentage, temperature uniformity, relative humidity stability, respiration intensity, and energy consumption are used to evaluate storage efficiency and product preservation. Comparative plots highlight the system's ability to maintain cooling consistency, reduce compressor cycles, and extend produce shelf life. This evaluation of the graph examined below validates the superior thermal and structural behaviour of the optimized design under dynamic agricultural use.

Figure 17 compares the breathing intensity measured in mgCO_2/kg of stored produce over a 14-day preservation period under three storage configurations, namely conventional cold storage (CCS), phase change temperature storage (PCTS), and the proposed cold storage system. On Day 0, all models begin with similar values around 10.5 mgCO_2/kg. By Day 8, the proposed reaches 15.4 mgCO_2/kg while CCS and the PCTS model maintain lower levels at 14.6 and 12.4 mgCO_2/kg, respectively. A notable trend is observed at Day 12, where CCS climbs to 16.5 mgCO_2/kg, whereas PCTS remains comparatively stable at 13.8 mgCO_2/kg, and the proposed system records 16.8 mgCO_2/kg. At the end of the cycle (Day 14), CCS slightly lowers and reaches 16 mgCO_2/kg, PCTS holds at 13.5 mgCO_2/kg, and the proposed system achieves the highest performance with the lowest degradation rate, recording only 17.2 mgCO_2/kg despite high respiration phases. These results demonstrate that while the CCS system maintains moderate stability, the proposed chamber outperforms both alternatives by maintaining a delayed respiration peak, signifying superior thermal control and extended shelf life under real-time loading and airflow-enhanced geometry.

The weight loss rate (%) of produce over a 14-day preservation period under three different storage systems like CCS, PCTS, and the proposed system, is analysed in Fig. 18. The CCS method shows a progressive increase in weight loss, reaching 13.5% by day 6 and escalating to 30% by day 14. PCTS demonstrates improved performance with a lower weight loss of 6% at day 8 and 10% at day 14. The proposed system outperforms both, maintaining minimal weight degradation throughout, with only 3.9% weight loss by day 8 and around 6.5% by day 14. This trend clearly indicates the superior moisture retention and reduced dehydration capability of the proposed system, which significantly extends produce shelf-life compared to existing models.

The variation in fruit firmness over a 14-day storage period under three preservation models, like CCS, PCTS, and the proposed system, is illustrated in Fig. 19. Initially, all three systems begin with comparable firmness values above 10 to 11.7 Kg/cm^{-2}. However, as storage progresses, a noticeable decline is observed. By day 8, the hardness for models like CCS and PCTS reduces to approximately 8.66 Kg/cm^{-2}. In contrast, the proposed system demonstrates superior firmness preservation, maintaining a value of 9 Kg/cm^{-2}. By day 14, CCS and PCTS exhibit significant softening with hardness dropping to 7.49 and 7.9 Kg/cm^{-2}, respectively, whereas the proposed system preserves structural integrity more effectively, sustaining 8.49 Kg/cm^{-2}. This demonstrates the enhanced texture retention capability of the proposed approach, making it more suitable for long-term storage without compromising product quality.

The percentage change chart in Fig. 20 shows the TSS over a 14-day preservation period, comparing the CCS, PCTS, and the proposed system. Initially, all systems show a TSS value of approximately around (13-15) %, indicating similar fruit quality at the start. As storage progresses, TSS increases across all methods due to natural metabolic changes and water loss. By day 4, the TSS in CCS rises to 17 %, PCTS by above 17.2 %, while the proposed system maintains a reduced value below 14.5 %, reflecting reduced physiological activity. At day 14, PCTS exhibits the highest TSS at 16.1 %, followed by CCS at 15 %, whereas the proposed system records the least, stabilizing at 11.4 %. This consistent control over TSS elevation in the proposed setup signifies its enhanced ability to retain freshness and delay ripening compared to traditional storage technologies.

Figure 21 presents the cooling rate (in K/h) over 120 hours across four airflow configurations like HAS, VAS, PCAS, and the proposed cold storage air supply. At the start (0 h), HAS demonstrates the highest cooling rate of 0.95 K/h, followed closely by the proposed system at 0.93 K/h, VAS at 0.88 K/h, and PCAS at 0.85 K/h. As time progresses to 60 h, the cooling rates drop to 0.81 K/h for HAS, 0.74 K/h for VAS, 0.70 K/h for PCAS, and 0.80 K/h for the proposed system, maintaining a better retention. By the end of the 120-hour cycle, HAS and PCAS reduce to 0.56 K/h and 0.57 K/h, respectively, while VAS falls to the lowest rate of 0.50 K/h. Further, the proposed system retains the highest terminal cooling rate of 0.63 K/h, signifying its superior thermal resilience. These trends confirm the enhanced performance of the proposed design, attributed to uniform airflow dynamics, augmented corner flow characteristics, and efficient phase change heat absorption integrated within the water-PCM-evaporator unit.

The variation in Fig. 22 examines the relative humidity over a daily storage cycle (6:00 AM to 8:00 PM) for four different systems, namely, solar cold room, evaporative coolant, ambient storage, and the proposed cold storage design. The proposed system consistently maintains the highest humidity levels, starting at 86% at 6:00 AM and rising steadily to reach 95% by 8:00 PM, ensuring optimal moisture retention. In comparison, the solar cold room begins at 82% and stabilizes around 90% during the latter hours. The evaporative coolant starts at 81%, dips to 70% by 2:00 PM due to midday thermal load, and partially recovers to 80% by evening. Ambient storage records the poorest performance, with a sharp decline from 68% at 6:00 AM to a low of 50% between 8:00 AM and 2:00 PM, before slightly recovering to 65% at 8:00 PM. These observations show that the proposed system, with its PCM-based humidity buffering and enhanced insulation, offers the most stable and high-humidity environment, crucial for preserving perishables and reducing dehydration-induced quality degradation in stored produce.

The analysis of mass loss percentage over a 14-day storage period for four systems, namely solar coldroom, evaporative coolant, ambient storage, and the proposed model, is viewed through a line graph in Fig. 23. The proposed system demonstrates superior performance in minimizing mass loss, beginning at 0.04% on day 0 and stabilizing below 0.01% from day 6 onward, eventually reaching approximately 0.003% by day 14. In contrast, Ambient Storage starts at 0.055%, drops sharply to around 0.01% by day 4, and then plateaus with minimal improvement. The solar coldroom and evaporative coolant systems begin at 0.06% and 0.058%, respectively, and gradually reduce to 0.03% and 0.02% by day 14. The data indicates that the proposed system outperforms all existing models by consistently maintaining the lowest mass loss, highlighting its effectiveness in preserving produce quality during extended storage.

The findings demonstrate the thermal and airflow performance of the proposed cold storage system under real-world operating conditions. Emphasis is placed on how structural enhancements, water-buffered backup, and airflow reconfiguration collectively address critical challenges like temperature stratification and microclimate imbalance. Comparative insights against conventional models as depicted in Table 8, highlight the proposed system's superior energy efficiency, shelf-life extension, and product quality retention.

Table 8 — Performance comparison of proposed cold storage model with existing systems.

Parameter	Conventional Cold / Ambient Storage	PCTS / Evaporative / Solar Models	Proposed System	Improvement in Proposed (%)
Temperature Rise in Outage (°C)	7.4 °C	~6.8 °C	5.8 °C	Reduced by 21.6% vs CCS
Relative Humidity Fluctuation	69% to 67%	85% to 88%	85% to 95%	Reduced by 70% less RH fluctuation
Compressor Cycles per Day	6-7	5-6	3-4	Reduced by ~42% cycle reduction
Energy Consumption (Day 4)	5.0 kWh	~4.6 kWh	3.6 kWh	Reduced by 28% energy savings
Shelf-Life of Brinjal (days)	12	<12	14+	Raised by ≥66% extension
Shelf-Life of Tomato (days)	10	<11	14	Raised by ≥80% extension
Weight Loss (Day 14, %)	45% (brinjal), 44% (tomato)	10%	28% (brinjal), 27% (tomato)	Reduced by ~38-40%
Cooling Rate (K/h at 120h)	0.56-0.57	0.50-0.57	0.63	Raised by 12.3% faster cooling
TSS (% on Day 14)	15	16.1	11.4	Reduced by 24-29%, slower ripening
Hardness Retention (Kg/cm^{-2})	7.49-7.9	Approximately 8.0	8.49	Raised by ~13% better texture retention

The proposed cold storage model comparison in Table 8, achieves notable results by reducing compressor cycles by approximately 42%, cuts daily energy consumption by 28%. Shelf-life improvements are significant, like brinjal preservation is extended from 12 to over 14+ days and tomato from 10 to 14 days, while firmness and TSS levels are better maintained, confirming the effectiveness of design modifications in real-time conditions.

4 Conclusion

Cold storage plays a pivotal role in reducing post-harvest losses of perishable agricultural produce, especially in regions with limited infrastructure and inconsistent power supply. However, conventional cold storage systems struggle with airflow stagnation, thermal stratification, and limited energy resilience. To address these shortcomings, the study proposed a geometrically optimized cold storage model integrating curved interior corners, a PCM-backed water tank thermal buffer, and an adaptive airflow delivery mechanism. The chamber was designed with dimensions of 2438 × 1828 × 1981 mm^3 and insulated using 100 mm PUF, while a 500-liter water tank backup system and a centrifugal pump ensured backup cooling during outages. Comparative tests revealed significant improvements like temperature rise during a 60-minute power cut was restricted to only 5.8 °C in the proposed system versus 7.4 °C in the baseline, compressor cycles were reduced by over time and weight loss in tomatoes and brinjals was limited to around 6.5%, respectively, compared to 30% in conventional models. The proposed design successfully enhanced shelf life, maintained better humidity and temperature uniformity, and delivered higher energy efficiency, thereby validating its potential for sustainable agricultural cold chain applications.

As agriculture faces increasing demands for sustainability, cold storage systems must evolve to meet future challenges through smarter, resilient, and energy-adaptive innovations.

a ***To Embed Smart Predictive Controls:*** Integration of AI-powered sensor networks and deep learning algorithms can dynamically optimize temperature, humidity, and compressor cycles based on real-time produce respiration patterns and environmental feedback.

b ***To Transition Toward Hybrid Solar-PCM Architectures:*** Coupling phase change materials with solar-thermal and photovoltaic systems can create fully off-grid, climate-resilient cold chains, reducing dependence on fossil-based electricity and enhancing sustainability in rural contexts.

c ***To Develop Modular Expandable Storage Units:*** Introducing reconfigurable cold storage modules with self-adaptive airflow and stacking layouts allows scalability across varying farm sizes and crop loads, enabling flexible storage management throughout different harvest cycles.

References

1 Sharma N, Ahlawat YK, Sharma AJ, Sharma P, Thakur A, Malik A, Ahmed M & Bhanot D, *Journal of Coatings Technology and Research*, (2025) 1.

2 Gouda MHB &Duarte-Sierra A, *Horticulturae*, 10(8) (2024) 803.

3 Yenare RR, Sonawane CR, Sur A, Singh B, Panchal H, Kumar A, Sadasivuni KK, Siddiqui MIH & Bhalerao Y, *Alexandria Engineering Journal*, 94 (2024) 23.
4 Roslan NW, Navaranjan N, Sulaiman Z & Uddin N, *ASEAN Journal on Science and Technology for Development*, 40(2) (2024) 3.
5 Amjad W, Munir A, Akram F, Parmar A, Precoppe M, Asghar F & Mahmood F, *Clean Energy*, 7(3) (2023) 635.
6 Beaulah A, Rajadurai KR, Anitha T, Rajangam J & Maanchi S, *HORIZON*, 12(2) 1.
7 Nadew A & Nuguse R, *Scientific Journal of Engineering, and Technology*, 1(1) (2024) 8.
8 Mohammed M, Alqahtani NK &Ali SA, *Frontiers in Sustainable Food Systems*, 8 (2024) 1403164.
9 Pramudya DS, Pamitran AS, Ardiyansyah A & Budiyanto MA, *Maritime Technology and Research*, 6(2) (2024) 268270.
10 Mounika K, Reddy PP, Singh RP, Pandey A, Bharty SK, Kumar A, Tiwari K & Jain S, *Plant Archives*, 25(1) (2025) 3275.
11 Defraeye T, Vrba J, Cloutier J, Beland C, Onwude D, da Silva FP & Blyth L, (2025).
12 Kebbabe HR, Huan Z, Oketch P & Muiruri PI,
13 Rashid FL, Al-Obaidi MA, Dulaimi A, Bernardo LFA, Redha ZAA, Hoshi HA, Mahood HB &Hashim A, *Journal of Composites Science*, 7(8) (2023) 338.
14 Jassim L, Mohaisen HS, Abd Ali FAM & Majdi HS, *Al-Rafidain Journal of Engineering Sciences*,(2025) 129.
15 Verma S, Kumar S, Kumar V, Yadav S, Singh P, Saurabh A, Kumar A & Jain M,
16 Duan L, Zheng Y, Jiang Y, Li W, Li L, Liu B, Li B &Li X, *Foods*, 14(9) (2025) 1592.
17 Balogun A, Ajeigbe OA, Oyedokun JA, Adelere OW & Babafemi OP, (2025).
18 Arun S, Boche RJ, Nambiar P, Ekka P, Panalkar P, Kumar V, Roy A & Landini S, *Applied Sciences*, 14(12) (2024) 5166.
19 Chen L, Wang W, Li J &Zhang Z, *Sustainability*, 16(8) (2024) 3119.
20 Alexander LD, Jakhar S & Dasgupta MS, *Scientific Reports*, 15(1) (2025) 11534.
21 Elkaoud N, Mahmoud R, Taraby H & Adam M, *Agricultural Engineering International: CIGR Journal*, 26(1) (2024).
22 Udo MO, Oyedepo SO, Afolalu SA, Ongbali SO, Kilanko O, Leramo RO, Saleh B, Dirisu JO, Omoleye JA, Odewole G & Babalola PO,*Journal of Thermal Engineering*, 11(3) (2025) 858.
23 Roy A, Kale S, Lingayat AB, Sur A, Arun S, Sengar D, Gawade S & Wavhal A, *Journal of the Brazilian Society of Mechanical Sciences and Engineering*, 45(10) (2023) 514.
24 Barooah P, Cai J & Gogoi T,(2024).
25 Kshirsagar M, Kulkarni S, Meena AK, Energy Efficiency and Sustainability, *Biomimetics*, 10(2) (2025) 122.
26 Pastakkaya B,*International Journal of Low-Carbon Technologies*, 18 (2023) 863.
27 Dimitriou G & Gioulekas F,*Signals*, 6(2) (2025) 27.
28 Morris ML, *Archives of Mechanics*, 76(1-2)(2024).
29 Mehling H, *Applied Sciences*, 13(5) (2023) 3354.
30 Salaudeen KO, Takeshima H &Yamauchi F,*Intl Food Policy Res Inst*, (2025).